UNPUBLISHED PRELIMINARY DATA

September, 1964

Report ESL-R-207
M.I.T. Project DSR 9459
Research Grant NSG-149-61

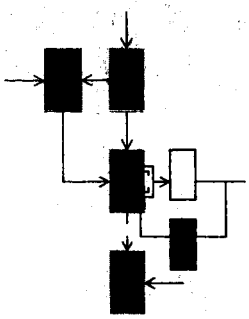

ZERO-RATE ERROR IN A VIBRATORY DOUBLE-MODULATION GYROSCOPE

Joseph A. D'Appolito

Electronic Systems Laboratory

MASSACHUSETTS INSTITUTE OF TECHNOLOGY, CAMBRIDGE 39, MASSACHUSETTS

Department of Electrical Engineering

September, 1964 Report ESL-R-207 Copy 2

ZERO-RATE ERROR IN A VIBRATORY DOUBLE-MODULATION GYROSCOPE

by

Joseph A. D'Appolito

The research reported in this document was supported, in part, by the National Aeronautics and Space Administration under Research Grant NSG No. 149-61. This report is published for technical information only and does not represent recommendations or conclusions of the sponsoring agency. Reproduction of this report, in whole or in part, is permitted for any purpose of the United States Government.

Approved by: George C. Newton, Jr.
George C. Newton, Jr.
Associate Director

Electronic Systems Laboratory
Department of Electrical Engineering
Massachusetts Institute of Technology
Cambridge, Massachusetts 02139

NOTICE

Requests for additional copies should be directed to:

National Aeronautics and Space Administration
Office of Scientific and Technical Information
Code AFSS-AD
Acquisition and Disseminations Branch
Washington 25, D. C.

ABSTRACT

15149

Cross-coupling between driven and sensed modes in a double modulation vibratory gyroscope is a known source of zero-rate output. An experimental double modulation vibratory gyroscope has, however, exhibited zero-rate error in excess of that attributable to cross-coupling alone. This report identifies additional major sources of zero-rate error in this gyroscope.

As a first step in the investigation a mathematical analysis is made of a square wave switching demodulator in which distinct random noises are simultaneously present on both the input and reference signals, these noises being correlated. General expressions for the demodulator output autocorrelation function and power density spectrum are obtained under the assumption that the noises are jointly Gaussian and subject only to the restriction that the reference signal-to-noise ratio be large.

Suspected noise sources and the mechanisms through which they are coupled into the signal processing electronics are then postulated, and using the above analysis, the resultant zero-rate output they would produce is predicted. This study indicates that noise induced in the sensing element by mechanical vibration produced during double modulation constitutes a second major source of zero-rate error. The study also shows that demodulator reference signal noise does not produce significant zero-rate output.

Finally, the results of an experimental investigation of additional sources of zero-rate output are presented. The most important result of this section is a determination of the frequency spectrum of the sensing element's zero-rate output before demodulation which permits confirmation of analytical predictions and an exact identification of two additional sources of zero-rate error.

ACKNOWLEDGEMENT

This report is based on a thesis submitted to the Department of Electrical Engineering at Massachusetts Institute of Technology in partial fulfillment of the degree of Master of Science.

The author gratefully acknowledges the supervision and guidance of Professor George C. Newton, Jr. Financial support under Research Grant NSG No. 149-61 from the National Aeronautics and Space Administration is also acknowledged.

CONTENTS

LIST OF FIGURES

CHAPTER I

INTRODUCTION

A. BACKGROUND

The Electronic Systems Laboratory at Massachusetts Institute of Technology has been investigating the use of double modulation as a means of reducing zero-rate error in vibratory drive, vibratory output gyroscopes. A major source of zero-rate output in practical vibratory gyroscopes is unavoidable cross-coupling between the driven and sensed vibrations caused by mass unbalance, force unbalance, and other imperfections. Double modulation, obtained by an additional rotation or vibration of the sensing element, separates the driven and sensed frequencies in such a manner that non acceleration dependent cross-coupled vibrations are not present at the sensed frequency. Thus, in theory, a large reduction in zero-rate error may be realized with double modulation.

An experimental vibratory gyroscope capable of operation with or without double modulation has been constructed using a double tuning fork as the sensing element.[1*] Double modulation is obtained by spinning the tuning fork about an axis of symmetry in the plane of vibration of the tines. Preliminary results indicate that double modulation reduces zero-rate error by roughly a factor of 100. However, the zero-rate output now contains substantial stochastic noise. A double modulation zero-rate output of 60 eru[**] was measured. Of this amount only 40 eru was due to the acceleration of gravity, and could be predicted theoretically.

It is clear that the ultimate source of the remaining stochastic zero-rate error is the random vibrational energy developed when the tuning fork package is spun at the double modulation frequency. The research reported herein was concerned with identifying the mechanism (s) by which this energy is introduced into the signal processing electronics and determining both analytically and experimentally the resultant zero-rate output noise produced.

---

* Superscripts refer to numbered items in the Bibliography.

** An eru is an earth rate unit equal to an angular velocity of 15°/hour.

The analytical and experimental program to be described was completed in three major steps. First, a fairly general mathematical description of a class of demodulators was obtained in which correlated random noise simultaneously corrupts both the input and reference signals. Next, probable noise sources and coupling mechanisms were postulated for the experimental double modulation gyroscope and a semi-quantitative analogy between the preceeding analysis and the gyroscope signal processing electronics was developed which provided useful information on the effect of the postulated noise sources on zero-rate output. Finally, these last results served as a guideline for intelligent experimental investigation of the sources of zero-rate output in the actual experimental device.

B. EQUIPMENT DESCRIPTION

The relationship between the tuning fork package and the signal processing electronics is shown in Fig. 1.1. Tuning fork vibration is maintained and stabilized by a closed-loop system consisting of an amplifier, tuning fork drive coils, the tuning fork, and the reference signal pickup coils. Vibratory output of the tuning fork is sensed by a capacitive transducer which is supported by a high Q resonant suspension system tuned to the sensed frequency, ω_s. The vibration detector signal is demodulated twice, first with respect to the tuning fork frequency, ω_d, and secondly with respect to the double modulation frequency, ω_m, to obtain a signal proportional to the applied angular rate.

C. NOISE SOURCES

From consideration of Fig. 1.1 there appear to be two paths whereby the random vibrational energy of rotation is most easily coupled into the signal processing chain. One path is directly through the output vibration sensor and the second is through the tuning fork reference signal pickup coils. In the first path noise from the double modulation carriage bearings passes through the resonant suspension system to the vibration detector where it is added to the desired signal. In the second path noise is produced by random relative motion between the tuning fork tines and the reference signal pickup coils and manifests itself as a noise signal superimposed upon the first demodulator reference signal. In the succeeding

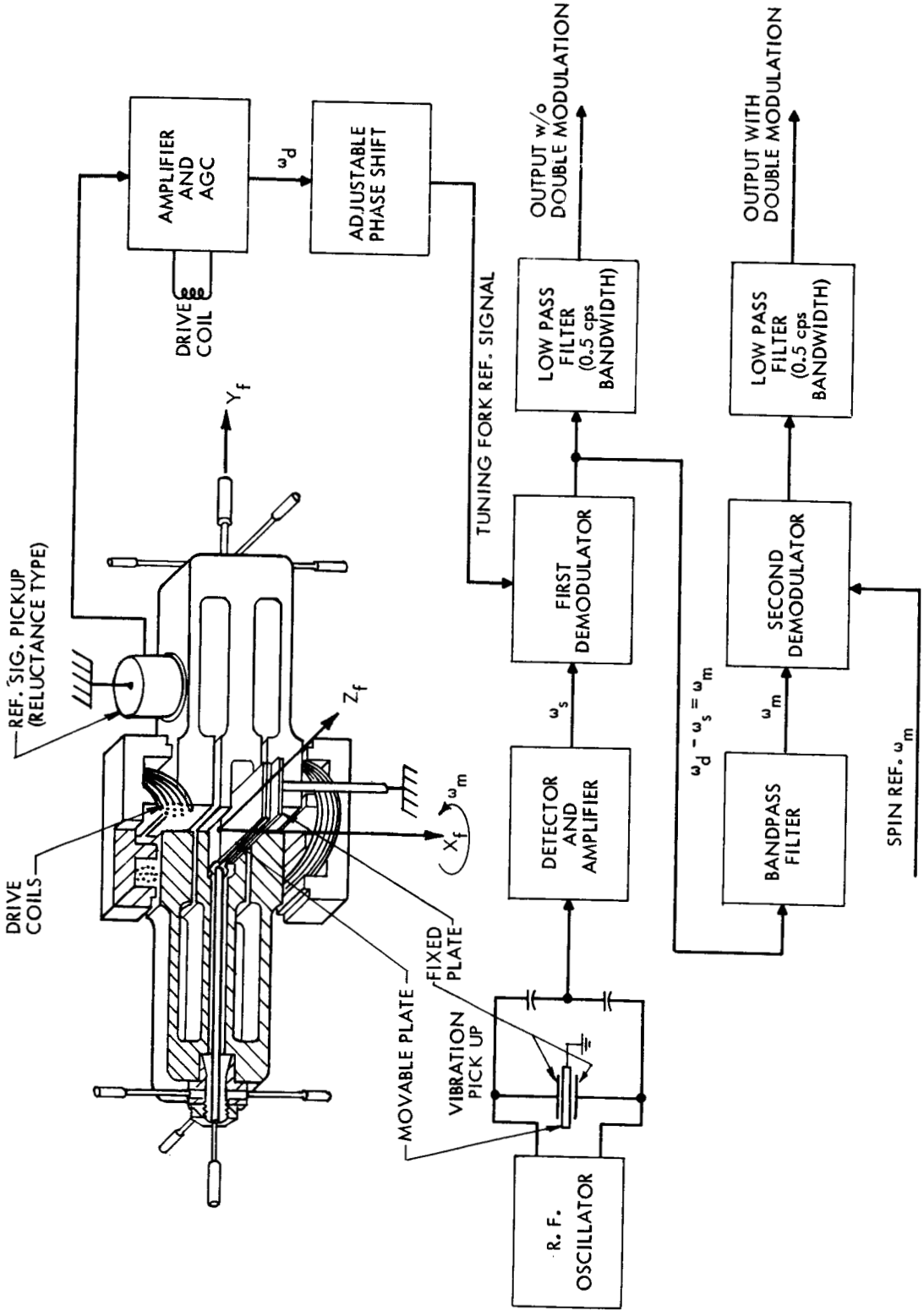

Fig. 1.1 Block Diagram of the Gyroscope's Electronics

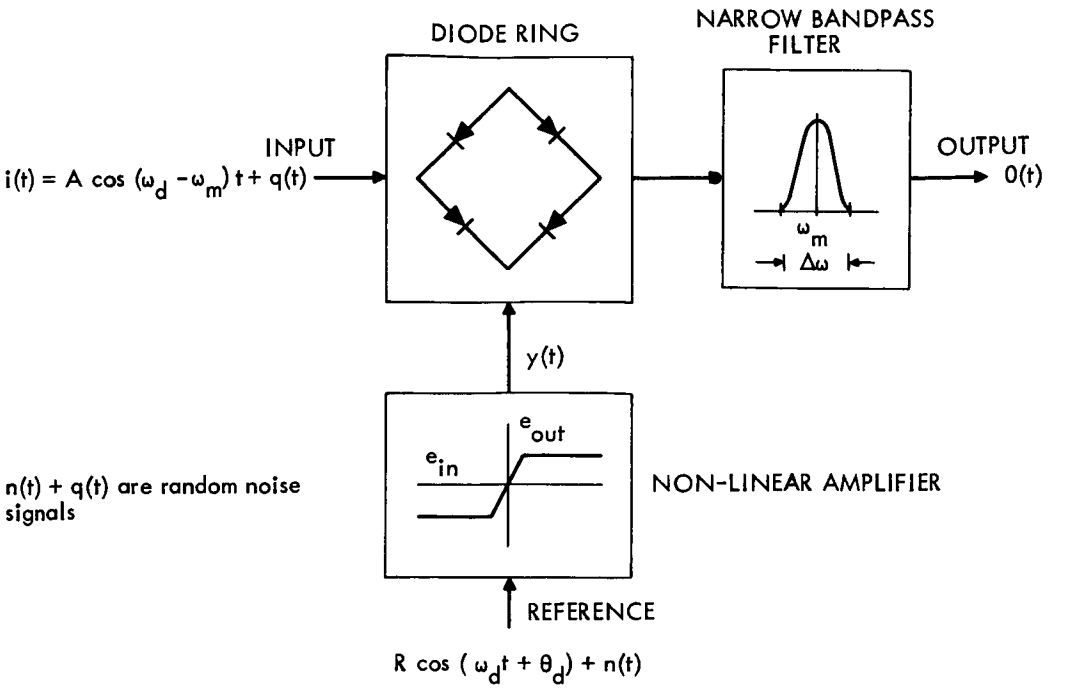

Fig. 1.2 Block Diagram of the First Demodulator

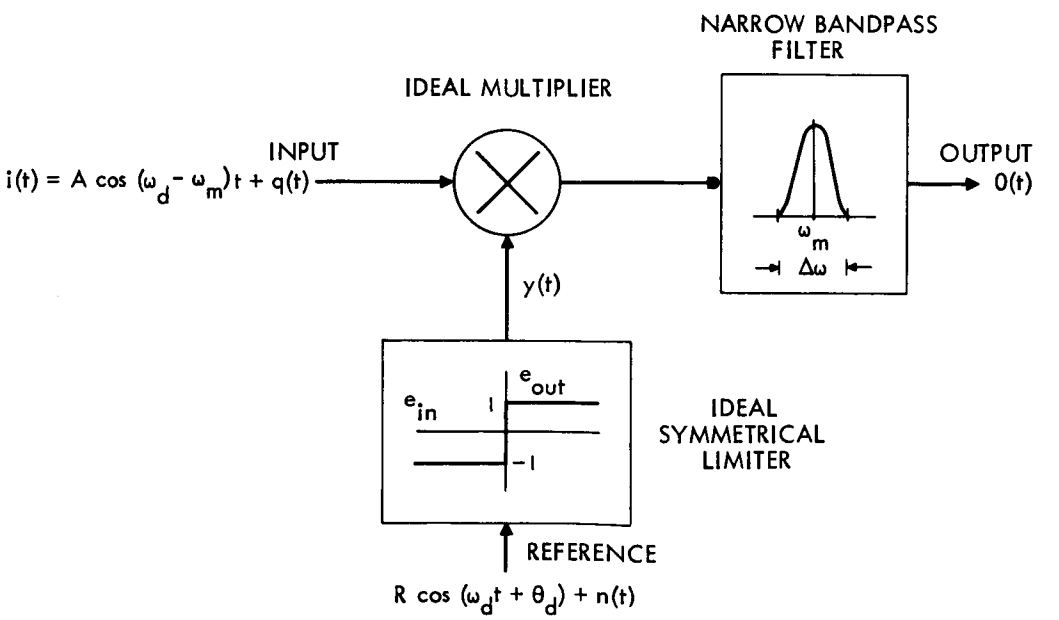

Fig. 1.3 Analytical Model of the First Demodulator

analysis only the above noise signals are considered. It is assumed, however, that they are correlated.

In view of the preceeding restriction it is seen that the second demodulator merely performs the function of frequency translation and does not of itself contribute to the zero-rate error. The following analysis will therefore be concerned only with a description of signal processing up through the first demodulator output.

D. MODEL SELECTION

The first demodulator, shown in Fig. 1.2, uses a conventional diode ring configuration. A square wave switching voltage is obtained for the diode ring by passing the sinusoidal reference signal through a highly non-linear amplifier. A narrow bandpass filter centered at ω_m follows the diodes.

The non-linear amplifier acts like a symmetrical limiter, while the diode ring performs the function of multiplication. For purposes of analysis the non-linear amplifier and diode ring combination will be replaced with an ideal symmetrical limiter and an ideal multiplier respectively as shown in Fig. 1.3. Experimental verification of the validity of this model has been obtained.[2]

CHAPTER II

DEMODULATOR ANALYSIS

A. INTRODUCTION

The analytical work presented in this report has a two-fold purpose. The first is to obtain a fairly general mathematical description of the output of a class of demodulators represented by Fig. 1.3 when correlated random noise signals are simultaneously present on both the reference and input signals The second purpose is to use the above analysis to explain the observed zero-rate output of an experimental double modulation vibratory gyroscope.

B. ANALYSIS

A general solution to the demodulator problem given arbitrary statistics for $n(t)$ and $q(t)$ is extremely difficult. If, however, the random variables are assumed wide sense stationary and jointly Gausian, and if it is further assumed that the reference signal-to-noise ratio is large, a relatively simple analysis can be accomplished in two steps. First, a time domain expression for the limiter output, $y(t)$, is obtained in terms of $R(t)$ and $n(t)$. This $y(t)$ is then used to find the demodulator output, its auto-correlation function and power density spectrum. Justification for the above assumption lies in the utility of the results obtained.

As a preliminary step in obtaining $y(t)$ it is instructive to find the limiter output for a deterministic input. This study will provide some initial familiarity with limiter action and thereby lead us more directly to the answer in the stochastic case.

To this end let us find the limiter output when its input is

$$A_m \left[\cos(\omega_d t + \theta_d) + a\cos(\omega_n t + \theta_n)\right]$$

where $a \ll 1$. Here ω_d may be considered the desired reference frequency, while ω_n represents a "noise" frequency. θ_d and θ_n are arbitrary phase angles. The limiter output is obtained simply by dividing the input by the instantaneous value of its envelope. That is

$$y(t) = \frac{A_m \left[\cos(\omega_d t + \theta_d) + a(\cos \omega_n t + \theta_n)\right]}{A_m \left\{1 + a^2 + 2a \cos\left[(\omega_d - \omega_n)t + (\theta_d - \theta_n)\right]\right\}^{1/2}}$$

$$= \cos(\omega_d t + \theta_d) + \frac{a}{2} \cos(\omega_n t + \theta_n) - \frac{a}{2} \cos\left[(2\omega_d - \omega_n)t + (2\theta_d - \theta_n)\right]$$

$$+ \text{ terms in higher powers of a.} \qquad (2.1)$$

Equation 2.1 contains much useful information. Notice first that though the amplitude of the interfering signal is suppressed relative to the reference signal by a factor of two, the phase of both signals is undisturbed. Secondly, observe that the first significant cross-modulation term involves the second harmonic of the reference signal and not its fundamental as one might first suspect. Equation 2.1 was obtained directly by series expansion and the use of trigonometric identities. Nothing in the analysis limits the form θ_d and θ_n. The results are true even if they are random functions of time. The analysis is easily extended to include any number of additional small amplitude sinusoidal noise signals. As in the simple case above each noise amplitude is reduced by a factor of two while the phase angle remains undistorted.

The validity of Eq. 2.1 has been confirmed experimentaly using the actual first demodulator of the experimental gyroscope for values of $a \leq 0.25$.

Turning now to the stochastic problem, a mathematical expression for those components of $y(t)$ which are significant in the demodulation process is desired. In Reference (2) it is shown that the autocorrelation function of the output of an ideal symmetrical limiter given the input $R \cos(\omega_d t + \theta_d) + n(t)$, where $n(t)$ is a stationary zero mean Gausian random process is

$$\phi_{yy}(\tau) = \sum_{m=0}^{\infty} \sum_{\substack{k=0 \\ m+k \\ \text{ODD}}}^{\infty} \frac{\epsilon_m h^2_{mk}}{k!} \phi^k_{nn}(\tau) \cos m\omega_d \tau \qquad (2.2)$$

where $\phi_{nn}(\tau)$ = autocorrelation function of $n(t)$

$$\epsilon_m = \begin{cases} \text{Newman number} \\ 1 \text{ for } m=0 \\ 2 \text{ all other } m \end{cases} .$$

The coefficients h_{mk} are evaluated using the formula

$$h_{mk} = \left(\frac{R}{N}\right)_\rho^{\frac{m}{2}} \frac{{}_1F_1\left[\frac{m+k}{2}; m+1; -\left(\frac{R}{N}\right)_\rho\right]}{m!\,\Gamma\left[1 - \frac{m+k}{2}\right]\left(\frac{\sigma^2}{2}\right)^{k/2}} \tag{2.3}$$

where $\left(\frac{R}{N}\right)_\rho$ = reference signal-to-noise power ratio

σ^2 = variance of n(t)

${}_1F_1(\alpha;\beta;-z)$ = confluent hypergeometric function defined by the series

$${}_1F_1(\alpha;\beta;-z) = \sum_{r=0}^{\infty} \frac{(\alpha)_r z^r}{(\beta)_r r!} = 1 + \frac{\alpha}{\rho}\,\frac{z}{1!} + \frac{\alpha(\alpha+1)}{\beta(\beta+1)}\,\frac{z^2}{2!} + \cdots$$

Putting Eq. 2.3 in 2.2 and noting that $\phi_{nn}^k(0) = \sigma^{2k}$ the total average power in y(t) becomes

$$\phi_{yy}(0) = \sum_{\substack{m=0 \\ m+k \text{ odd}}}^{\infty} \sum_{k=0}^{\infty} P_{mk} = \sum_{\substack{m=0 \\ m+k \text{ odd}}}^{\infty} \sum_{k=0}^{\infty} \frac{\epsilon_m h_{mk}^2}{k!}\,\sigma^{2k}$$

$$= \sum_{\substack{m=0 \\ m+k \text{ odd}}}^{\infty} \sum_{k=0}^{\infty} \frac{\epsilon_m\, 2^k \left(\frac{R}{N}\right)_\rho^m {}_1F_1^2\left[\frac{m+k}{2}; m+1; -\left(\frac{R}{N}\right)_\rho\right]}{k!(m!)^2\,\Gamma^2\left[1 - \frac{m+k}{2}\right]} \tag{2.4}$$

Evaluation of the terms P_{mk}^3 shows that for reference signal-to-noise power ratios of twenty or more the total average power in y(t) is given with little error by

$$\phi_{yy}(0) \cong \sum_{\substack{m=1 \\ m \text{ odd}}}^{N} P_{m0} + P_{01} + P_{21} \quad , \tag{2.5}$$

this approximation improving rapidly with increasing reference signal-to-noise power ratio (N is a small number chosen such that $P_{N0} < P_{01}$ or P_{21}). It follows from Eq. 2.5 that the autocorrelation function of y(t) is given approximately by

$$\phi_{yy}(\tau) \approx \sum_{\substack{m=1 \\ m \text{ odd}}}^{N} 2h_{m0}^2 \cos m\omega_d \tau + h_{01}^2 \phi_{nn}(\tau) + 2h_{21}^2 \phi_{nn}(\tau) \cos 2\omega_d \tau \tag{2.6}$$

and y(t) must therefore have the form

$$y(t) \cong \sum_{\substack{m=1 \\ m \text{ odd}}}^{N} 2h_{m0} \cos(m\omega_d t + \phi_m) + h_{01}\, n(t) + 2h_{21}\, n(t) \cos(2\omega_d t + \theta) \tag{2.7}$$

Setting the phase angle of the reference signal equal to zero and recalling the limiter properties derived from equation 1.1, it is seen that the portion of y(t) of importance in the demodulation process is simply

$$y(t) = 2h_{10} \cos \omega_d t + h_{01} n(t) + 2h_{21}\, n(t) \cos 2\omega_d t \, . \tag{2.8}$$

Observe that as in the deterministic case the first significant cross-modulation term involves the second harmonic of the reference signal. The amplitude ratios predicted by Eqs. 1.1 and 1.8 are also consistent. For instance for an input signal-to-noise power ratio of twenty Eq. 2.1 says the output power ratio equals $4(\frac{1}{2}) = 4 \times 20 = 80$. Using Table 2.1 of reference (2) it is seen that for the stochastic case

$$\left.\frac{P_{10}}{P_{01}}\right|_{\substack{=80 \\ (\frac{R}{N})_\rho = 20}}$$

Equation 2.8 was derived using Gausian statistics for $n(t)$. Its consistency with Eq. 2.1, however, indicates that Eq. 2.8 is probably a good approximation to $y(t)$ for many non-Gausian disturbances also.

With a valid expression for $y(t)$ the demodulator output given the input $A\cos(\omega_d - \omega_m)t + q(t)$ is found to be

$$\begin{aligned} 0(t) &= i(t)y(t) = Ah_{10}\cos\omega_m t + Ah_{10}\cos(2\omega_d - \omega_m)t \\ &+ 2h_{10}q(t)\cos\omega_d t + Ah_{01}n(t)\cos(\omega_d - \omega_m)t \\ &+ h_{21}An(t)\cos(3\omega_d - \omega_m)t + Ah_{21}n(t)\cos(\omega_d + \omega_m)t \\ &+ (h_{01} + 2h_{21}\cos 2\omega_d t)\,q(t)\,n(t) \quad . \end{aligned} \tag{2.9}$$

The output autocorrelation function and power density spectrum follow directly from Eq. 2.9 and are given below:

$$\begin{aligned} \phi_{oo}(\tau) &= \frac{(Ah_{10})^2}{2}\cos\omega_m\tau + h_{10}^2\,\phi_{qq}(\tau)\cos\omega_d\tau \\ &+ \frac{(Ah_{01})^2}{2}\phi_{nn}(\tau)\cos(\omega_d - \omega_m)\tau + \frac{(h_{21}A)^2}{2}\phi_{nn}(\tau)\cos(3\omega_d - \omega_m)\tau \\ &+ \frac{(Ah_{21})^2}{2}\phi_{nn}(\tau)\cos(\omega_d + \omega_m)\tau \\ &+ \left[h_{01}^2 + \frac{h_{21}^2}{2}\cos 2\omega_d\tau\right]\left[\phi_{nn}(\tau)\,\phi_{qq}(\tau) + \phi_{nq}(\tau)\,\phi_{qn}(\tau)\right] \end{aligned} \tag{2.10}$$

and

$$\Phi_{oo}(\omega) = \frac{(Ah_{10})^2}{4}\left[u_o(\omega - \omega_m) + u_o(\omega + \omega_m)\right]$$

$$+ \frac{h_{10}^2}{2}\left[\Phi_{qq}(\omega-\omega_d) + \Phi_{qq}(\omega+\omega_d)\right]$$

$$+ \frac{(Ah_{01})^2}{4}\left[\Phi_{nn}(\omega-\omega_s) + \Phi_{nn}(\omega+\omega_s)\right]$$

$$+ \frac{(h_{21}A)^2}{4}\left[\Phi_{nn}(\omega+2\omega_d+\omega_s) + \Phi_{nn}(\omega-2\omega_d-\omega_s)\right]$$

$$+ \frac{(Ah_{21})^2}{4}\left[\Phi_{nn}(\omega-\omega_d-\omega_m) + \Phi_{nn}(\omega+\omega_d+\omega_m)\right]$$

$$+ h_{01}^2\left[\Phi_{nn}(\omega) * \Phi_{qq}(\omega) + \Phi_{nq}(\omega) * \Phi_{qn}(\omega)\right]$$

$$+ \frac{h_{21}^2}{4}\left[u_o(\omega+2\omega_d) + u_o(\omega-2\omega_d)\right] * \left[\Phi_{nn}(\omega) * \Phi_{qq}(\omega) + \Phi_{nq}(\omega) * \Phi_{qn}(\omega)\right] \tag{2.11}$$

where the symbol (*) signifies the operation of convolution. Terms in Eqs. 2.10 and 2.11 whose spectra obviously fall outside the output filter passband have been dropped.

It should be noted that expressions 2.10 and 2.11 are relatively simple because all cross-correlation functions of any two terms in Eq. 2.9 are identically zero. This is true primarily because the signal frequency and the reference frequency are not equal. The steps in the analysis of the more common synchronous case (i.e., $\omega_m \equiv 0$) are identical to those of the preceeding analysis, but one must take care to include the now non-zero cross-correlation terms.

C. APPLICATION

It now remains to apply Eqs. 2.10 and 2.11 to the experimental double modulation vibratory gyroscope. In light of the introductory discussion Fig. 2.1 represents a reasonable model for the gyroscope's signal processing system up through the first demodulator output. Here $H_1(s)$ is the resonant suspension system transfer function, $H_2(s)$ represents the output filter, and $H_3(s)$ and $H_4(s)$ are linear filters which account for the two different

paths through which random vibrational energy passes into the system.

$H_3(s)$, $H_4(s)$, and $n(t)$ are not known. However, by making reasonable assumptions about their nature an analysis may be completed which will provide useful information about the effect of the postulated noise sources on zero-rate output. Consistent with this attitude the following assumptions are made:

$$H_3(s) = 1 \tag{2.12a}$$

$$H_4(s) = \beta > 1 \tag{2.12b}$$

$$\Phi_{nn}(\omega) = \frac{\sigma^2}{2\omega_d + \omega_m} \quad \text{for} \quad |\omega| < \omega_d + \frac{\omega_m}{2} \tag{2.12c}$$

$$= 0 \quad \text{elsewhere}$$

Since the results will now be only approximate, considerable simplification of the remaining calculations is obtained by replacing $H_1(s)$ and $H_2(s)$ with equivalent ideal filters shown in Fig. 2.2. Equivalence is here defined by the relationships:

$$|H_{1_{eq}}(\pm j\omega_s)| = |H_1(\pm j\omega_s)| \tag{2.13a}$$

$$\int_{-j\infty}^{j\infty} H_1(s)\, H_1(-s)\, ds = 2\,|H_{1_{eq}}(\pm j\omega_s)|^2\, \Delta\omega_1 \tag{2.13b}$$

where the various terms are defined in Fig. 2.2. The resonant suspension system transfer function is

$$H_1(s) = \frac{K}{s^2 + \frac{\omega_s}{Q_s}\, s + \omega_s^2} \tag{2.14}$$

where Q_s = suspension system Quality factor

ω_s = suspension system resonant frequency.

Putting Eq. 2.14 in 2.15 one obtains

$$H_{1_{eq}}(\pm j\omega_s) = \frac{KQ_s}{\omega_s^2} \tag{2.15a}$$

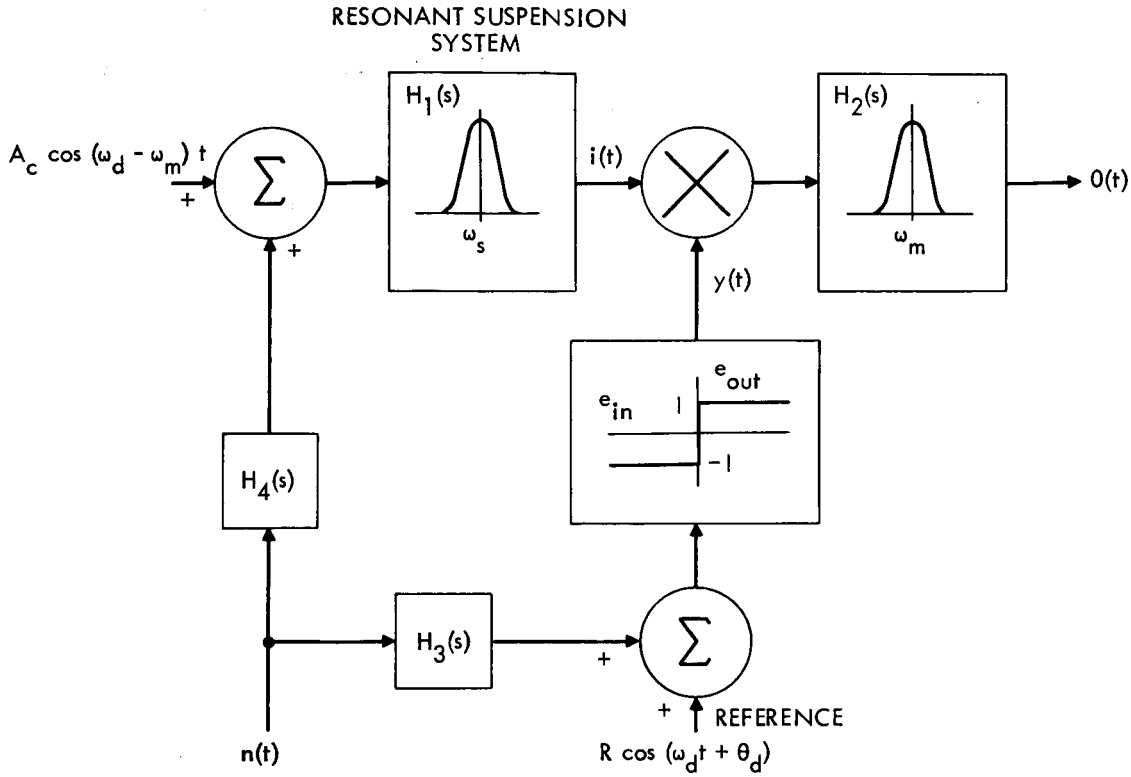

Fig. 2.1 Model of Gyroscope's Signal Processing System

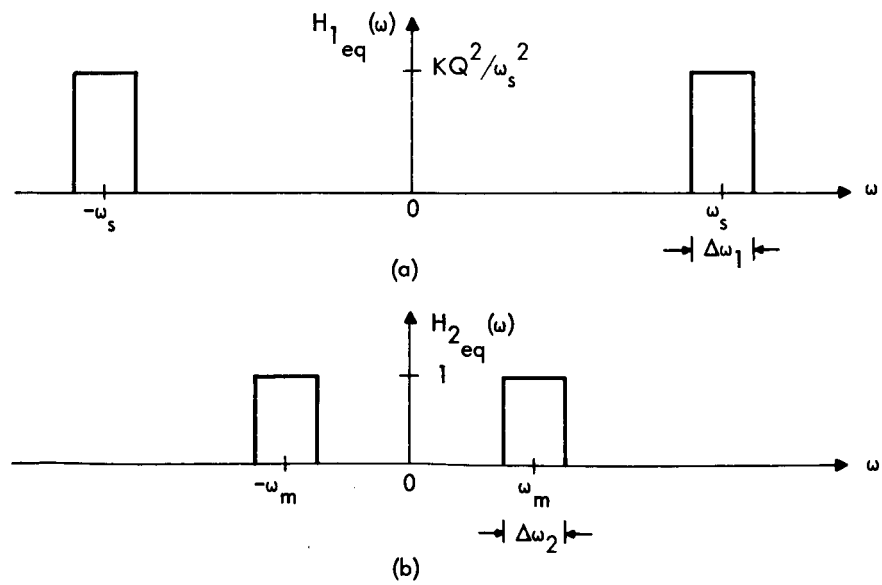

Fig. 2.2 Amplitude Response of Equivalent Filters

$$\Delta\omega_1 = \frac{\pi}{2}\frac{\omega_s}{Q_s} \tag{2.15b}$$

For the experimental gyroscope the equivalent ideal filter for $H_2(s)$ is simply

$$|H_{2_{eq}}(\pm j\omega_m)| = 1 \tag{2.16a}$$

$$\Delta\omega_2 = 2\pi \tag{2.16b}$$

The use of ideal filters will cause little error as long as $\Delta\omega_1 < \Delta\omega_2$, a condition which is fulfilled in the experimental apparatus.

Comparison of Figs. 1.3 and 2.1 yield the following relationships for the various terms in Eqs. 2.10 and 2.11:

$$A = \frac{A_c K Q_s}{\omega_s^2} \tag{2.17a}$$

$$\Phi_{nn}(\omega) = \Phi_{nn}(\omega) \tag{2.17b}$$

$$\Phi_{qq}(\omega) = \beta^2 |H_{1_{eq}}(\omega)|^2 \Phi_{nn}(\omega) = \frac{K^2 Q_s{}^2 \beta^2 \sigma^2}{\omega_s{}^4 (2\omega_d + \omega_m)}$$

$$\text{for } \omega_s - \frac{\Delta\omega_1}{2} < |\omega| < \omega_s + \frac{\Delta\omega_1}{2}$$

$$= 0 \text{ elsewhere} \tag{2.17c}$$

$$\Phi_{nq}(\omega) = \Phi_{qn}(\omega) = \beta |H_{1_{eq}}(\omega)| \Phi_{nn}(\omega) = \frac{K Q_s \beta \sigma^2}{\omega_s{}^2 (2\omega_d + \omega_m)}$$

$$\omega_s - \frac{\Delta\omega_1}{2} < |\omega| < \omega_s + \frac{\Delta\omega_1}{2}$$

$$= 0 \text{ elsewhere} \tag{2.17d}$$

The various power density spectra of Eqs. 2.11 are shown in Figs. 2.3*

*Spectra which fall completely outside output filter passband are not included in Fig. 2.4.

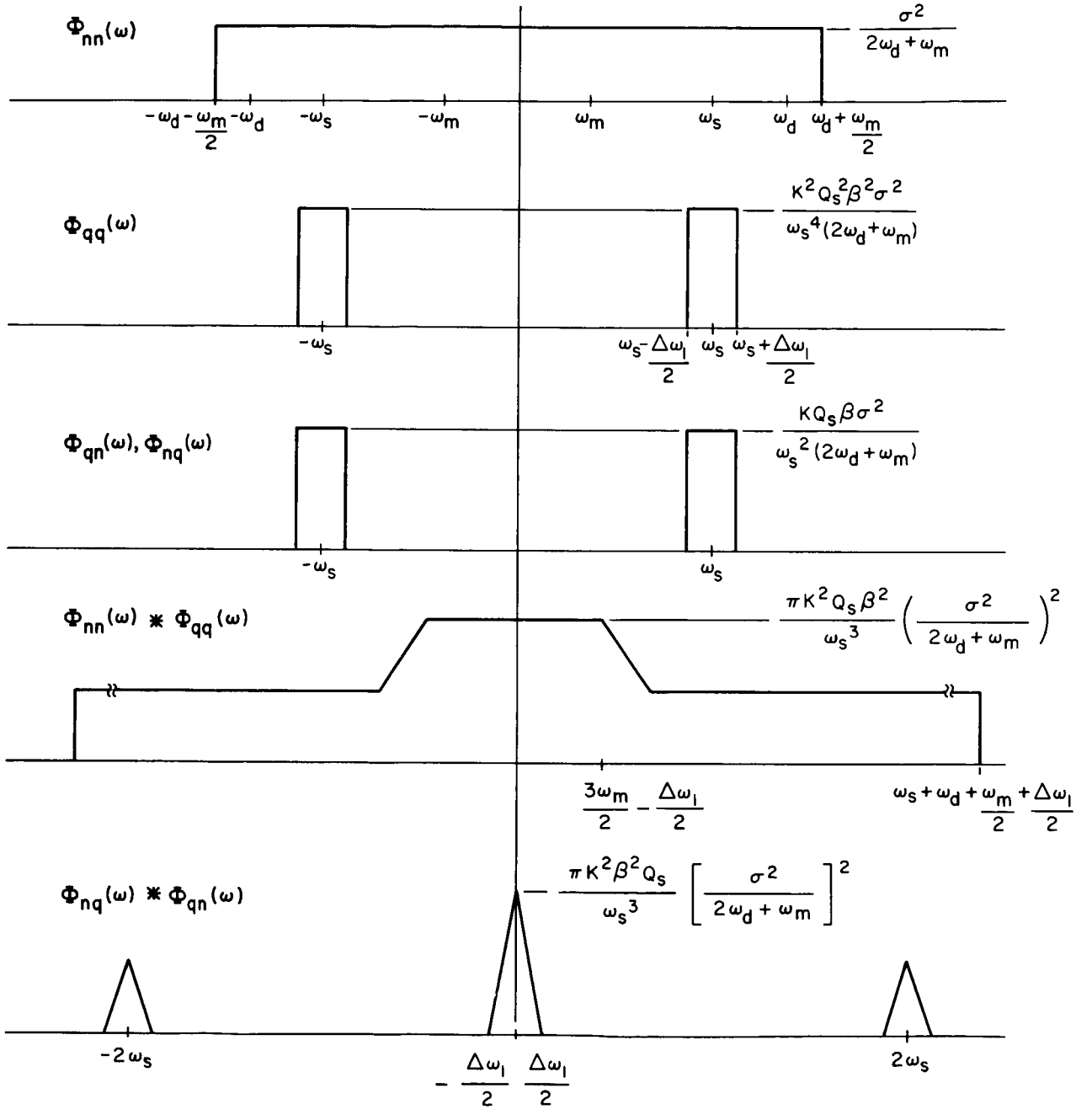

Fig. 2.3 Power Spectra of Equation 1.11

and 2.4. The demodulator output power spectrum is simply the sum of all spectra within the output filter passband each multiplied by the appropriate constants of Eq. 2.11. The total average output power is

$$P_o = \int_{-\infty}^{\infty} \Phi_{oo}(\omega)\, d\omega = \frac{h_{10}^2}{2}\left(\frac{A_c K Q_s}{\omega_s^2}\right)^2 + h_{10}^2 \frac{\pi K Q_s \beta^2}{\omega_s^3}\left(\frac{\sigma^2}{2\omega_d + \omega_m}\right)$$

$$+ \frac{1}{2}\left(h_{01}^2 + \frac{h_{21}^2}{2}\right)\left(\frac{\pi \omega_s}{Q_s}\right)\left(\frac{A_c K Q_s}{\omega_s^2}\right)^2 \left(\frac{\sigma^2}{2\omega_d + \omega_m}\right)$$

$$+ \left(h_{01}^2 + \frac{h_{21}^2}{4}\right)\left(\frac{\pi K}{\omega_s}\right)^2 \left(\frac{\sigma^2}{2\omega_d + \omega_m}\right)^2 \beta^2 \qquad (2.18)$$

The first term of Eq. 2.18 represents the zero-rate output power of the acceleration dependent cross-coupled signal. The second term is caused by the random noise in the vibration detector output. The third term is due to the interaction of the reference signal noise, n(t), with the reference and cross-coupled signals, and the fourth term is produced by the interaction of the vibration detector and reference signal noises.

In the experimental gyroscope $2\omega_d + \omega_m = 4500$. Thus for any reasonable value of noise power

$$\frac{\sigma^2}{2\omega_d + \omega_m} \ll 1 \qquad (2.19)$$

Also for reference signal-to-noise power ratios of 20 or more

$$h_{10}^2 \geq 100\left(h_{01}^2 + \frac{h_{21}^2}{2}\right) \qquad (2.20)$$

From Eqs. 2.19 and 2.20 it is clear that the third and fourth terms of Eq. 2.18 are respectively at least 100 times smaller than the first and second terms. Since the observed magnitudes of the cross-coupled and stochastic portions of the zero-rate output are comparable it appears that only the first two terms of Eq. 2.18 contribute significantly to zero-rate error.

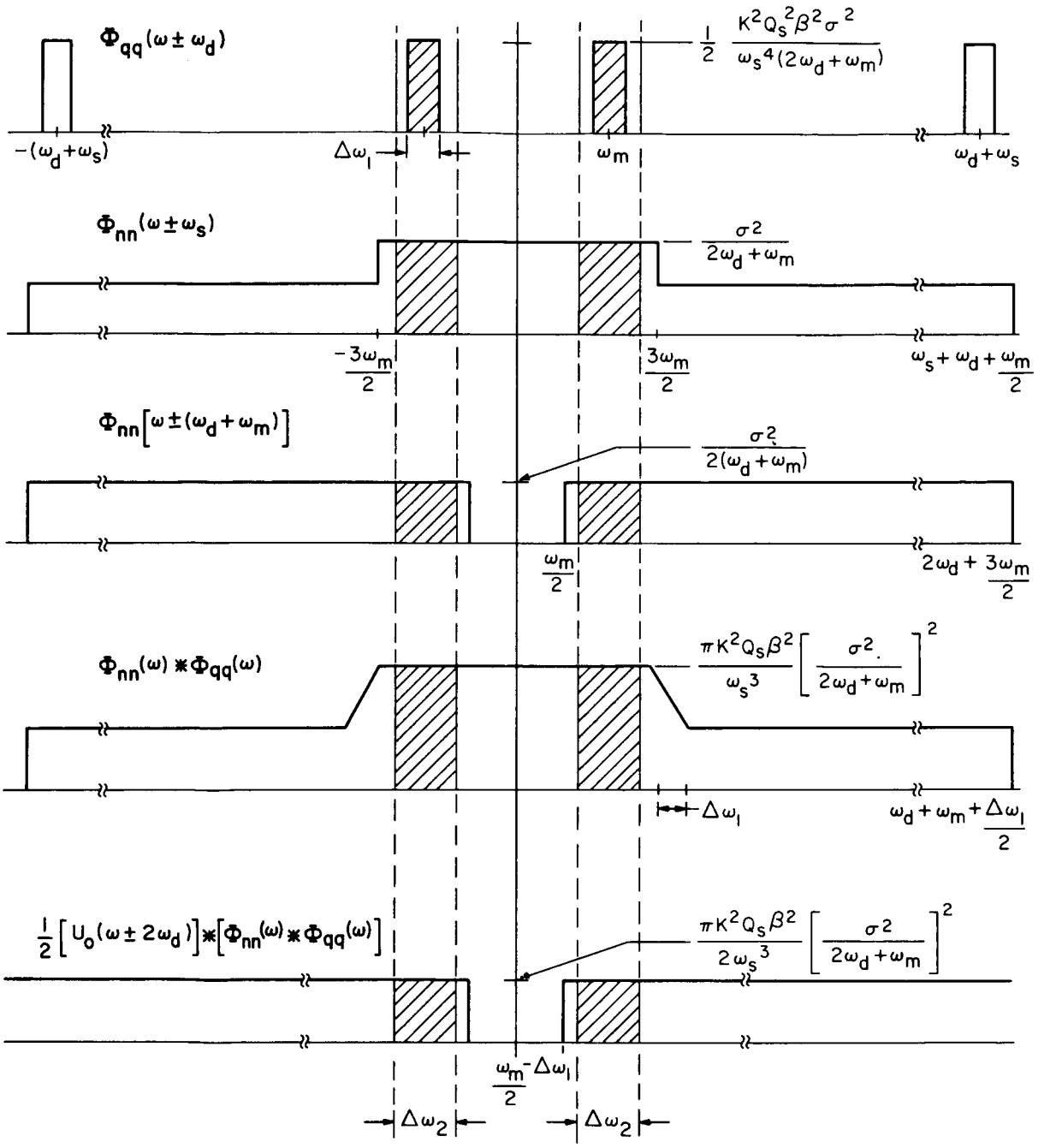

Fig. 2.4 Demodulator Output Spectra

The experimental program to be described in the next chapter was aimed at determining the presence and magnitude of each term in Eq. 2.18 and thereby confirming the presence of the postulated noise sources. Further discussion of Eq. 2.18 must await the presentation of the experimental results.

CHAPTER III

EXPERIMENTAL RESULTS

A. INTRODUCTION

The major experimental effort was aimed at verifying the presence of the two noise sources postulated in Chapter I. To do this two separate experiments were conducted. In the first experiment the first demodulator was placed in operation with its noisy reference signal and a pure sinusoidal input. Cross-modulation products in the output spectrum were then determined. The second consisted of measuring the vibration detector output spectrum with the tuning fork package spinning and the tuning fork off.

B. VIBRATION DETECTOR NOISE

As part of the continuing research and concurrent with the analytical work of this thesis, the original tapered roller bearings on the double modulation carriage were replaced with conical journal bearings in order to evaluate the effect of the latter on zero-rate output. Unfortunately, due to machining errors and case distortions produced by machining, the zero-rate noise increased by nearly a factor of 1000 over the levels cited in Chapter I. A quick check of the vibration detector output spectrum showed it to be rich in harmonics of the spin frequency. In order to conduct a meaningful experiment under these highly degraded conditions spin harmonics had to be kept far from the suspension resonance.

The spin frequency of the experimental double modulation gyroscope is continuously variable over a range of 5 - 50 cps. Within this range 30 cps was chosen since it provided a wide symmetrical spread of spin harmonics about the suspension resonance of 314 cps, while keeping vibration detector saturation low.

Figure 3.1 shows a block diagram of the experimental set-up for determining the vibration detector output spectrum. The reference oscillator was varied over a range of 20 - 500 cps. Random output of fairly uniform amplitude was observed up to about 300 cps where the peak-to-peak amplitude began to rise. Concentrating on the frequency near

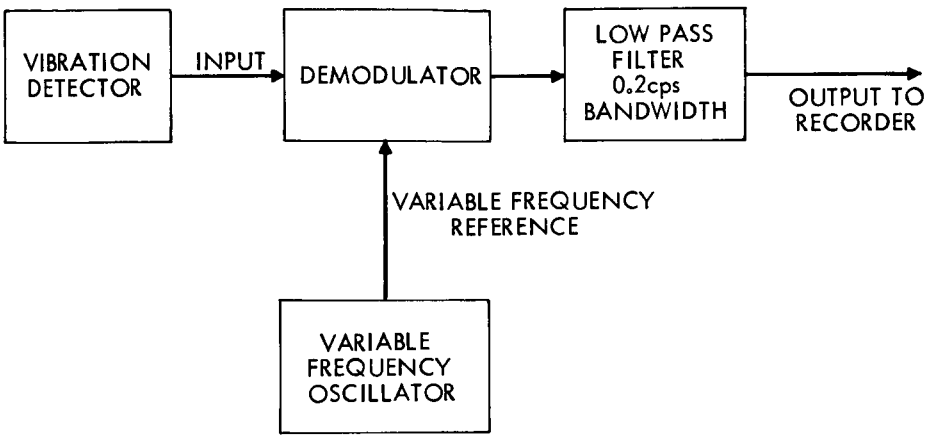

Fig. 3.1 Experimental Set-up for Determining the Output Spectrum of the Vibration Detector

suspension resonance, the reference oscillator was swept several times from 310 to 318 cps at a slow uniform rate of approximately 0.1 cps per second. Two records typical of these sweeps are shown in Fig. 3.2. In each case, as the suspension system resonant frequency was approached the apparent frequency* of the random output decreased rapidly while the d.c. level rose. As the reference oscillator crossed resonance the apparent frequency equaled the sweep rate, indicating an essentially d.c. output. Using earlier calibration data the measured d.c. level corresponds to approximately 1000 eru.

Above 320 cps random output fell rapidly, reaching its low frequency amplitude at about 350 cps and falling to residual levels above 400 cps.

In addition to the random output all harmonics of the spin frequency up through the eleventh were observed in the vibration detector output spectrum. At this point the tuning fork was energized to measure the zero-rate output due to cross coupling. These data are given in Table 3.1.

*Apparent frequency as used here is equivalent to the number of zero crossings per second.

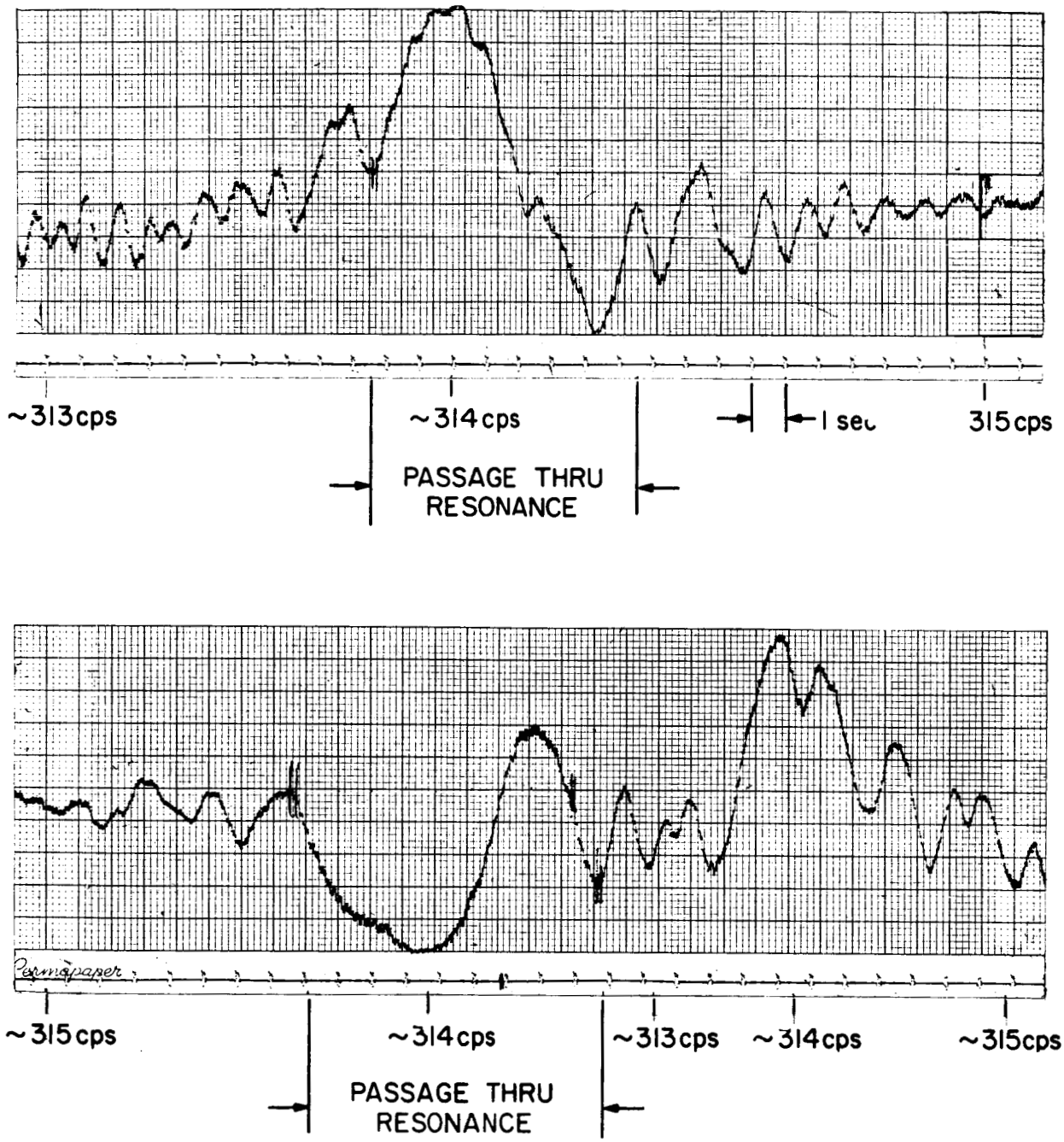

Fig. 3.2 Frequency Sweep through Suspension System Resonance

Table 3. 1

Periodic Components of Vibration Detector Zero-Rate Output

Components of Vibration Detector Output	Frequency (cps)	Amplitude (Relative Units)* Tuning Fork Off	Tuning Fork On
Spin Harmonics	30	4.0	4.0
	90	0,8	0.8
	120	1.0	1.0
	210	0.4	0.4
	240	0.6	0.6
	270	4.8	4.8
	300	4.0	4.0
	330	9.6	9.6
Cross-Coupled Component	328.5	0.0	6.7

*1 Unit ≈ 1000 eru

C. REFERENCE SIGNAL NOISE

Without double modulation the tuning fork reference signal has a peak-to-peak amplitude of 4 volts. Figures 3. 3a and 3. 3b are photographs showing the random fluctuations of the reference signal amplitude during double modulation. The scale is 0. 2 volts per centimeter and only the uppermost portion of the reference signal appears on the trace. These photographs show that the reference signal amplitude variation during double modulation rarely exceeds five percent of the single modulation amplitude.

Because of this relatively small reference noise amplitude complete spectral analysis of the corrupted reference signal using the technique outlined in the preceeding section was not possible with available equipment. An estimate of the noise power in the corrupted reference signal was obtained, however, by noting that as the reference signal-to-noise ratio decreases the fundamental-to-second harmonic ratio of the periodic portion of the reference signal increases. Using Table 2. 2 of reference (2) the

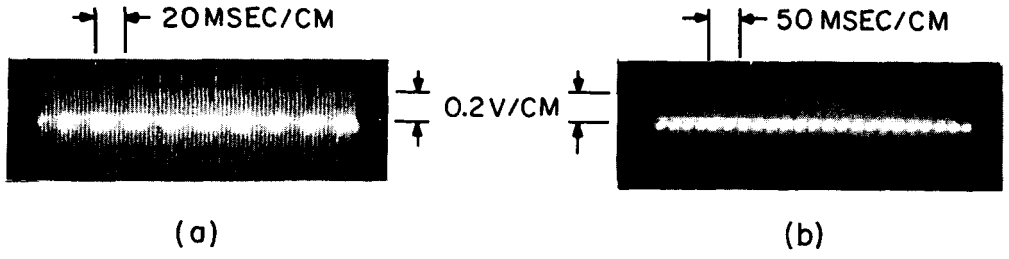

VERTICAL SENSITIVITY 0.2V/CM
(BRIGHT HORIZONTAL TRACE IS SPIN REFERENCE SQUARE WAVE)

Fig. 3.3 Photographs of Reference Signal and Superposed Noise

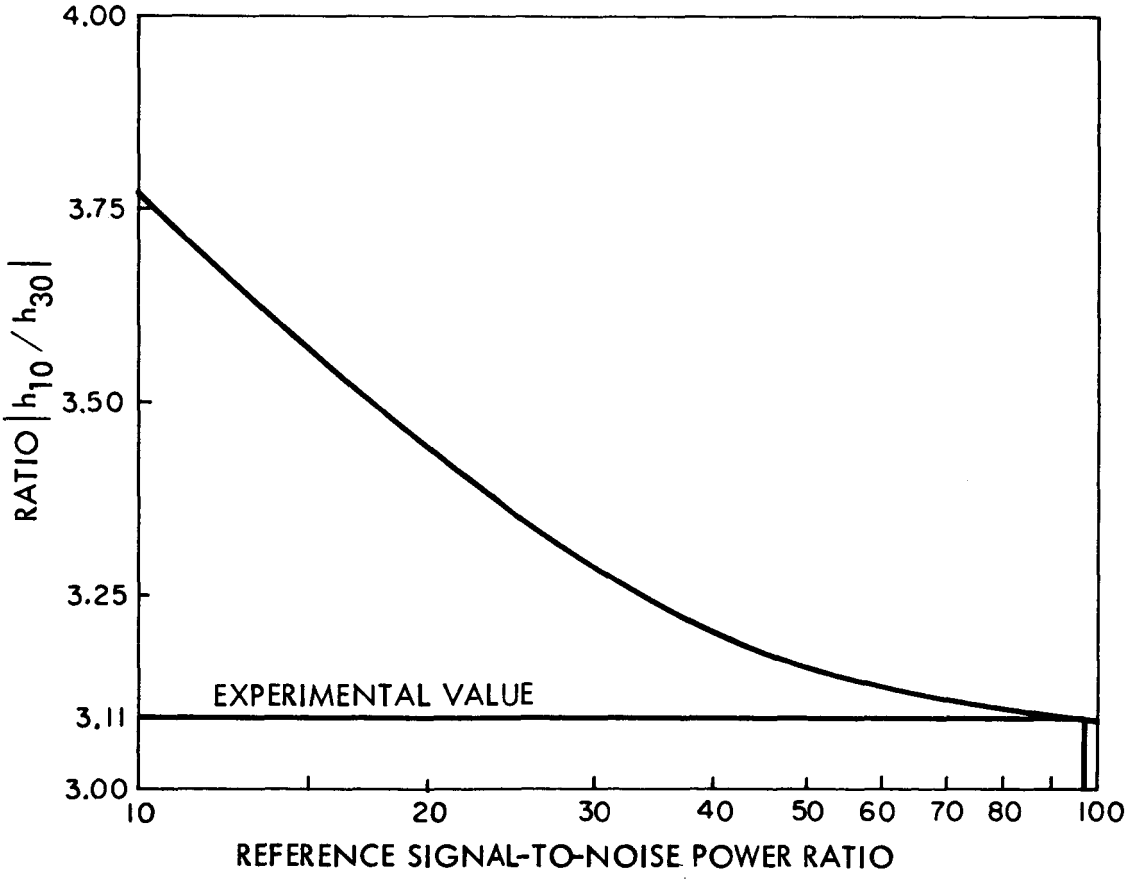

Fig. 3.4 Plot of $|h_{10}/h_{30}|$ Versus Reference Signal-to-Noise Ratio

ratio of h_{10} to h_{30} is plotted versus reference signal-to-noise power ratio in Fig. 3.4. The measured amplitude ratio during double modulation is shown on Fig. 3.4. It is seen that

$$\left(\frac{R}{N}\right)_p = \frac{R^2/2}{\sigma^2} \simeq 100$$

Since $R = 2$ we have that

$$\sigma^2 \simeq 0.02$$

This result substantiates the assumption made in Chapter III, viz;

$$\frac{\sigma^2}{2\omega_d + \omega_m} << 1 \qquad (2.19)$$

As a final step in data taking the first demodulator was placed in normal operation. Photographs of the vibration detector and first demodulator outputs were obtained at spin frequencies of 30, 40 and 45 cps. These photographs are shown in Fig. 3.5. Figure 3.5d, taken prior to the bearing change, is included for comparison purposes.

At 30 cps the demodulator output contains components due primarily to cross coupling, the tenth and eleventh spin harmonics, and narrow band noise, all of which are approximately equal (see Table 3.1). Ideally, the vibration detector output should have the waveform of a sinusoidally modulated suppressed carrier signal. The lower trace of Fig. 3.5a shows the actual signal.

As resonant * operation was approached the spin harmonics also approached the suspensionsystem resonance and the vibration detector output rose rapidly. Figure 3.5b shows the condition at 40 cps. Here the eighth spin harmonic is 320 cps and the cross-coupled signal falls on 319 cps. Observe that these periodic components predominate and the output has lost most of its random character. Also note that the vibration detector is saturated more than half the time as indicated by the clipped

---

* Resonant operation is defined as $\omega_d - \omega_s = \omega_m$.

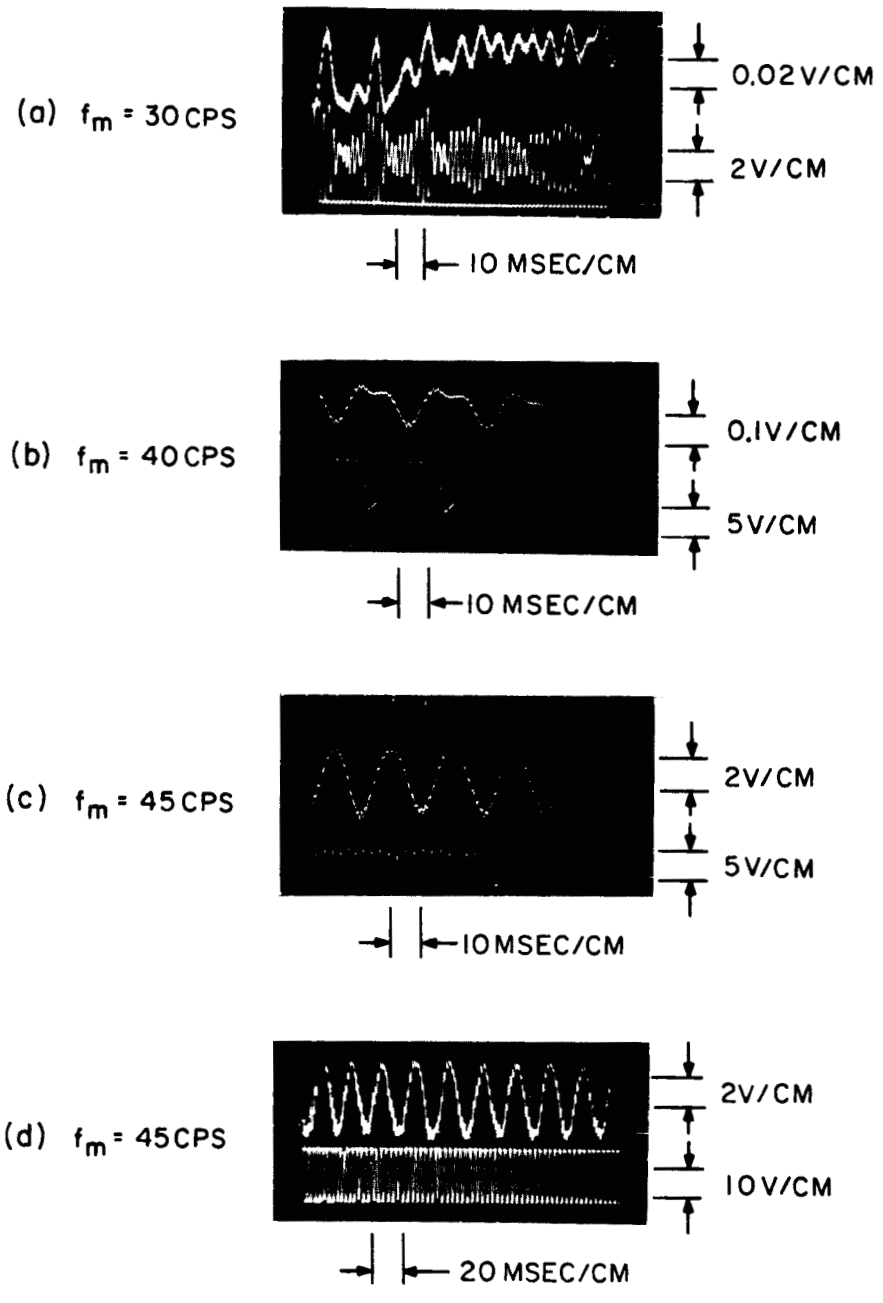

FOR ALL PICTURES:

UPPER TRACE - 1st DEMODULAR OUTPUT
LOWER TRACE - VIBRATION DETECTOR OUTPUT

Fig. 3.5 Output of Vibration Detector and First Demodulator During Double Modulation

trace. Finally at 45 cps the frequency of the cross-coupled component and the seventh spin harmonic coincide and both are essentially equal to the suspension resonant frequency. The vibration detector is fully saturated and the demodulator output is periodic at 45 cps. (The ripple on the demodulator output is caused by switching transients in the diode ring and residual unbalance of the reference switching voltage. In normal operation this ripple is filtered out.)

CONCLUSIONS AND RECOMMENDATIONS

At the present stage of development the major sources of zero-rate noise in the double modulation vibratory gyroscope in order of importance are:

1. Acceleration dependent cross-coupling
2. Spin frequency harmonics produced primarily by double modulation carriage shaft run-out.
3. Random vibrational energy produced by bearings and coupled into the vibration detector.

Again for the present instrument, first demodulator reference signal noise is not causing significant zero-rate error.

Methods of reducing the first source of error and ultimate limits on its magnitude are discussed elsewhere. The second two sources are increasing functions of the double modulation carriage vibration and the basic problem of reducing them is one of vibration reduction and vibration isolation.

The second source can be eliminated from the demodulator output by proper selection of ω_d, ω_s, and ω_m. For the present instrument ω_d is approximately 360 cps at a spin frequency of 48 cps. Lowering the suspension resonance, ω_s, to 312 cps the important spin harmonics will fall at 288 cps and 336 cps which are ±24 cps away from the suspension resonance. The spin harmonics will therefore be greatly attenuated by the suspension system and can be eliminated with a narrow band-pass filter at the demodulator output.

This step does not, however, eliminate the spin harmonic which can still saturate the vibration detector or drive it out of its linear range. And, of course, the third source of noise still remains. These two sources can only be reduced by reducing the level of carriage vibration and the

amount of this vibration coupled into the output detector.

Proper care in machining and balancing, and the use of precision ball bearings, coupled with the change in ω_s and ω_m outlined above should return noise levels to slightly below previous best performance.

Further reduction is probably most profitably obtained by studying suspension schemes for the tuning fork package which will provide additional vibration isolation in the 200 - 400 cps range, and especially near the suspension resonance.

BIBLIOGRAPHY

1. Bush, R. W., Newton, G. C. Jr., "Reduction of Errors in Vibratory Gyroscopes by Double Modulation" to be published in a forthcoming issue of IEEE Transactions on Automatic Control.

2. D'Appolito, J. A., "Zero-Rate Error in an Experimental Double Modulation Gyroscope," Massachusetts Institute of Technology, Electronic Systems Laboratory Master of Science Thesis, June, 1964.

3. Middleton, D. and Johnson, V., A Tabulation of Selected Confluent Hypergeometric Functions, Technical Report No. 140, Cruft Laboratory, Harvard University, Cambridge, Mass., 5 January 1952.